




Article

Cu@PtRu Core–Shell Nanostructured Electrocatalysts Anchored on Reduced Graphene Oxide toward Methanol Oxidation

Walber dos Santos Gomes ^{1,*} , Rodrigo della Noce ¹ , Tamires de Sousa de Matos ¹, Flávio Vargas Andrade ², Fábio Alberto Molfetta ¹  and José Pio Iúdice de Souza ¹

¹ Faculdade de Química, Instituto de Ciências Exatas e Naturais, Universidade Federal do Pará, Belém 66075-110, Brazil; dellanoce@ufpa.br (R.d.N.); tamires.mt.pro@gmail.com (T.d.S.d.M.); fabioam@ufpa.br (F.A.M.); jpiao@ufpa.br (J.P.I.d.S.)

² Faculdade de Ciências Exatas e Tecnológica, Universidade Federal do Pará, Abaetetuba 68440-000, Brazil; flaviovargas@ufpa.br

* Correspondence: walber.quimica@gmail.com; Tel.: +55-91980315867

Abstract: This work reports the influence of a reduced graphene oxide (rGO) support on the catalytic performance of Cu@PtRu/rGO electrocatalysts toward methanol oxidation in an acidic medium. These electrocatalysts are synthesized via a two-step reduction method; the first step utilizes ethylene glycol for the reduction of Cu²⁺ ions, forming Cu/rGO. In the second step, spontaneous redox reactions take place, in a process known as galvanic displacement, where the Pt²⁺ and Ru³⁺ species are reduced to form PtRu layers, and the copper is partially oxidized to the solution. Then, the Cu@PtRu/rGO core–shell is produced, comprising Cu in the inner structure (core) and PtRu on the outer part (shell). To compare the catalytic performance of the prepared nanocatalysts (NCs), Pt/C, PtRu/C, and Cu@PtRu/C are also synthesized on Vulcan XC-72R carbon. All catalysts are characterized via X-ray diffraction (XRD) and high-resolution transmission electron microscopy (HRTEM). Cyclic voltammetry (CV) and chronoamperometry (CA) are employed to measure the electrochemical performance. The core–shell/rGO combination is superior in catalytic activity to the traditional Pt/C, PtRu/C, and Cu@PtRu/C catalysts for the methanol oxidation reaction. These results suggest that Cu@PtRu/rGO exhibits a high bulk activity for methanol electrooxidation, a high stability, and a high tolerance to CO poisoning, meaning it is possible to reduce the platinum loading in proton-exchange membrane fuel cells (PEMFCs).

Keywords: electrocatalysts; core–shell; reduced graphene oxide



Citation: Gomes, W.d.S.; Noce, R.d.; de Matos, T.d.S.; Andrade, F.V.; Molfetta, F.A.; Iúdice de Souza, J.P. Cu@PtRu Core–Shell Nanostructured Electrocatalysts Anchored on Reduced Graphene Oxide toward Methanol Oxidation. *Energies* **2023**, *16*, 6508. <https://doi.org/10.3390/en16186508>

Academic Editor: Xia Lu

Received: 17 June 2023

Revised: 31 July 2023

Accepted: 18 August 2023

Published: 9 September 2023



Copyright: © 2023 by the authors. Licensee MDPI, Basel, Switzerland. This article is an open access article distributed under the terms and conditions of the Creative Commons Attribution (CC BY) license (<https://creativecommons.org/licenses/by/4.0/>).

1. Introduction

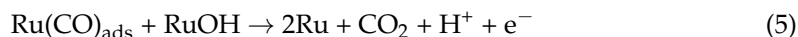
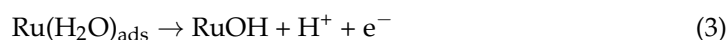
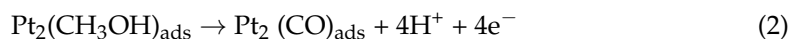
Direct-methanol fuel cells (DMFCs) are a type of device that directly convert the chemical energy of methanol into electricity. They have a higher volumetric energy density, and cost advantages, over cells that use hydrogen as fuel. Thus, DMFCs are promising candidates for an energy source for transportation and electronic devices [1–4]. However, the efficiency of fuel cells depends on appropriate catalysts in the electrodes [5–7]. In this sense, PtRu nanoparticles transported in carbonaceous materials are considered the best anodic catalyst for the electrooxidation of methanol [8–11]. Two issues limit the practical applications of the PtRu catalyst: the high cost of platinum, and the low resistance to catalytic poisons, i.e., mutated chemical species, originating from the partial transmission of methanol, which are adsorbed at the active sites of the Pt [12,13].

Recent research has sought to prepare catalysts with a low Pt content and a resistance to the catalytic poisons that impair the performance of DMFCs. The alternative found so far, to circumvent these issues, is to change the morphology of the nanoparticles in the catalysts. In this new arrangement, Pt is not inserted throughout the crystalline lattice of a nanoparticle, but forms an envelope in the core, composed of a metal or a low-cost metal alloy. These core–shell nanostructures are the most efficient way to reduce the use of

precious metals in electrocatalysts [10,14]. In the literature, the most common supports for these nanostructures are Vulcan XC-72R carbon and carbon nanotubes, with graphene and its derivatives (GO and rGO) mentioned in several technological applications. Despite the range of support materials for nanocatalysts, reduced graphene oxide (rGO) has a higher surface area, favoring a better dispersion of nanoparticles on its surface, a lower electronic resistivity and, consequently, a better electrocatalytic performance [15–19].

Our findings suggest that rGO is an excellent choice as a support for core–shell nanoparticles. The reasons are: (i) Cu is a low-cost material, its positive electrode potential renders it stable in an acid medium, in addition to its face-centered cubic crystalline structure (FCC), the same as Pt, favoring the epitaxial growth of platinum on the surface of its nanoparticles; (ii) PtRu is well known as the most promising alloy for anodic catalysis for methanol oxidation in an acidic medium; and (iii) catalysts supported on materials derived from graphene have a higher electrochemically active surface area, and a higher electronic conductivity, than those of other carbon materials [20–22].

The adsorption and oxidation of methanol occurs in few materials in an acidic medium—only in platinum and platinum alloys. In electrochemical systems, the point of interest is the oxidation of methanol on an anodic substrate. This process takes place in different stages, depending on the applied potential values [23–25]. Although it contains a single carbon atom in its molecule, methanol undergoes electrooxidation in the presence of PtRu electrocatalysts in a series of steps, as shown in the chemical equations below, suggested by different authors [26,27].



There are two relevant aspects of the mechanism of methanol oxidation at Pt sites. The first stems from the fact that the different crystallographic faces have different energies for the adsorption of methanol; the energetically more-favorable face on the surface, and the (111) face, are the sites of a higher adsorption of methanol molecules. The second is the occurrence of the sequential loss of protons, to give rise to a series of hydrogenated intermediates with multiple bonds that convert to linearly adsorbed CO, as explained by Hannet [26]. This evidence comes from the results obtained via DEMS (differential electrochemical mass spectrometry) and FTIR (Fourier transform infrared) [28,29].

To circumvent the problem of the poisoning of the catalyst with CO, two effects of the formation of a Pt metallic alloy of Pt and a second metal—in particular, with Ru—can be considered; the bifunctional mechanism and the electronic effect act together, leading CO to oxidize at low potentials [30–32]. In this context, this work aims to demonstrate the high efficiency of Cu@PtRu/rGO in the methanol electrooxidation reaction through the core–shell formation, a relatively low-cost method, in which copper partially replaces the expensive matrix of the Pt and Ru noble metals.

2. Materials and Methods

2.1. Preparation of Reduced Graphene Oxide (rGO)

The preparation of graphene oxide (GO) was based on the modified Hummers method [33,34]. To a 500 mL beaker, 0.1 g of graphene and 0.075 g of NaNO₃ were added, followed by 3.44 mL of concentrated sulfuric acid, under slow stirring, to avoid overheating. Subsequently, 0.450 g of KMnO₄ (KMnO₄, 100% Merck, Rio de Janeiro, Brazil) was added to the mixture, still under constant stirring, at room temperature. After all the KMnO₄ was

added, the reagents continued to be under constant agitation for 24 h. Then, 10 mL H₂SO₄ (5% *m/m*) was added and, after 2 h, 0.9 mL H₂O₂ (30% *m/m*). Due to the tendency of the stirring to stop, as the viscosity of the mixture increases with time, 40 mL of 30% *m/m* H₂SO₄ + 5% *m/m* H₂O₂ was slowly added, over the five days of synthesis. The formation of a yellowish suspension was observed, and a dark-brown material was deposited at the bottom of the vessel. To remove impurities, 30 mL of HCl (3%) was added to the suspension. The material was then washed extensively with ultrapure water. The obtained GO was placed in an oven to dry, at a temperature of 80 °C, for 12 h. The material synthesized previously was reduced to rGO in the first step of the synthesis of the electrocatalysts, the step that used ethylene glycol as a reducing agent for the cupric ions in the solution. The material obtained after the reduction process was Cu/rGO, which was then washed extensively with ultrapure water.

2.2. Preparation of Cu@PtRu/rGO Catalysts

Core-shell Cu@PtRu/C catalysts were prepared via a two-step reduction method. Two types of carbon support were used, Vulcan XC72R carbon and GO, respectively. In the first step, initially, 70 mg of carbon powder was suspended in a solution of 8 mL of ultrapure water (18.2 MΩ cm) and 2 mL of isopropyl alcohol, and stirred under sonication for 20 min. Then, 30 mg of Cu from a penta-hydrated copper sulfate solution (CuSO₄·5H₂O) and 2 mL of ethylene glycol were added to a beaker containing the previously prepared GO suspension. The pH was adjusted to 10 using potassium hydroxide/ethylene glycol solution (5% *w/w* KOH/EG), and the mixture was refluxed for 6 h, at 140 °C. Subsequently, the Cu/rGO system was filtered, washed excessively with ultrapure water, and placed in an oven for 12 h, at a temperature of 60 °C. In the second step of the synthesis for each catalyst, solutions with varying volumes of H₂PtCl₆·6H₂O and RuCl₃·xH₂O were used. The mass proportions were 16 mg of Pt and 8.3 mg of Ru in Cu@PtRu/C-16 and in Cu@PtRu/rGO-16 catalysts, 18 mg of Pt and 9.2 mg of Ru in Cu@PtRu/C-18, 30 mg of Pt and 15.2 mg of Ru in PtRu/C-30 and, finally, 30 mg of Pt in Pt/C-30. The samples were designated in relation to the Pt mass utilized in each catalyst preparation. In each synthesis, the volumes containing these masses were added to the Cu/C suspension, where the galvanic displacement process occurred. This final mixture was stirred for 15 min under sonication. After stirring, the pH value of the solution was adjusted to 8, via the adding of 0.1 mol L⁻¹ KOH. Then, the mixture was refluxed at 100 °C. After reflux, it was filtered, and the resulting Cu@PtRu/C was washed excessively with ultrapure water, to remove traces of the reducer or ions from the salt or acid. Finally, it was placed in an oven at 60 °C, for 12 h.

2.3. Physical Characterization

The catalysts were characterized via XRD and HRTEM. X-ray measurements were made using a PANalytical X-ray Diffractometer, model X'PERT PRO MPD (PW 3040/60) from Malvern Instruments Ltd., Westborough, Massachusetts, USA. A copper anode monochromatic X-ray beam (Kα 1.540598 Å) was used. The recordings were performed in the 2θ interval between 10 and 110°, at a scan of 2° per minute. The characteristic patterns in the samples were identified through comparison with patterns from a database that was developed by the Joint Committee on Powder Diffraction Standards (JCPDS). The HRTEM images were acquired in a transmission electron microscope, model TECNAI G2F2 (FEI Company, Hillsboro, OR, USA), operating at 200 kV beam power, in scan-transmission mode (STEM) for (high-angle annular dark-field) HAADF microanalysis and imaging.

2.4. Electrochemical Analyses

The electrochemical measurements were carried out using an Autolab PGSTAT12 Potentiostat/Galvanostat Electrochemical System (Metrohm company, Herisau, Switzerland). A glass electrochemical cell, without separation between the compartments, was used, with five openings at the top, through one of which a working electrode was introduced.

The counter electrode consisted of a platinum wire with a Pt plate in contact with the solution, and the reference electrode was Ag/AgCl/KCl(3M). The working electrode was a glassy carbon disk, with a geometrical area of 0.196 cm² (the glassy carbon electrode has a polished surface, so its surface area was assumed as the geometric area). The thin-film electrode was prepared as follows: 5 mg of catalyst was dispersed in 1 mL of isopropanol and 1 mL of water. Next, 60 μL of Nafion (0.25% Nafion) was added, and then the mixture was subjected to sonication for 15 min. Then, 60 μL of the dispersion was transferred to the glassy carbon disk, using a pipette, and finally, the electrode was placed in an oven, until complete drying was achieved. The catalysts were characterized via cyclic voltammetry (CV) and chronoamperometry (CA) tests at room temperature. The current densities were measured in terms of A.cm⁻², via the normalization of the electrochemical surface area of the electrode. Oxidation reactions (OR) were studied in 0.5 M H₂SO₄ solution, saturated with N₂ for 10 min. This method is used to compare the electrocatalytic activity of different electrodes, taking into account the number of surface active sites; i.e., it is an evaluation of the electrocatalytic activity intrinsic to the real area of these electrodes. The basis of this method is the fact that carbon monoxide molecules occupy, in principle, all active sites available for electrocatalytic reactions. The charge value of the conversion of CO_{ads} to CO_{2(g)} [Q_{CO(C)}] in microcoulombs (μC), divided by 420 μC, is numerically equal to the electrochemically active area (EAA), defined by Equation (6). The EAA values obtained for each electrode are used as the normalization factors for the currents that are now expressed in A.cm⁻² units. The CO amount is obtained via the integration of the voltametric peak (shaded area), as shown in Figure 1 [35].

$$\text{EAA} = \text{CO oxidation charge } (\mu\text{C}) / 420 (\mu\text{C} \cdot \text{m}^{-2}), \quad (6)$$

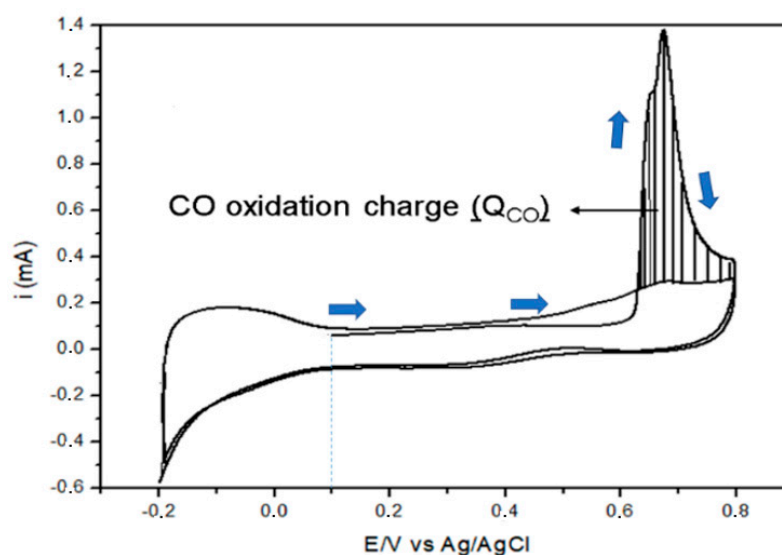


Figure 1. Cyclic voltammogram of the Pt/C-30 catalyst obtained in 0.5 M H₂SO₄ solution, at 20 mV/s. The shaded area represents the CO oxidation peak. The arrows in blue indicate the direction of the anodic scan.

3. Results

3.1. Characterization

3.1.1. X-ray Analyses

The Cu@PtRu/C structure is confirmed via XRD, which shows the partial core-shell formation for Cu@PtRu/C-16 and Cu@PtRu/C-18, and the full core-shell formation for Cu@PtRu/rGO-16 crystallites. These structures are a consequence of the substitution of atoms on the surface of Cu nanoparticles with Pt and Ru atoms. Figure 2 shows the XRD pattern for Pt/C-30, PtRu/C-30, Cu@PtRu/C-16, Cu@PtRu/C-18, and Cu@PtRu/rGO-16. For all PtRu-containing catalysts, there is a slight shift in relation to the Pt/C-30 diffraction

peak in the (111) plane. These shifts to values higher than 2θ are indicative of the formation of the PtRu alloy, either directly on the support, or in the Cu crystallites. The formation of PtRu can also be inferred from the values calculated for the lattice parameters of the PtRu catalysts that present lower values in relation to the monatomic Pt alloy. The first peak located at about $2\theta = 25^\circ$ for Pt/C-30, PtRu/C-30, Cu@PtRu/C-16, and Cu@PtRu/C-18 is associated with the face (002) of the crystal structure of the carbon. The absence of this peak is noted in the Cu/rGO and Cu@PtRu/rGO-16 catalysts, and it is associated with the efficiency of the exfoliation process of graphite sheets via the chemical route, as the exfoliation increases the distance between the constituent planes of the graphite, shifting 2θ to smaller values. The other three peaks at 40° , 47° , and 68° are associated with the (111), (200), and (220) planes, characteristic of the face-centered (fcc) cubic crystal alloys of Pt [36,37].

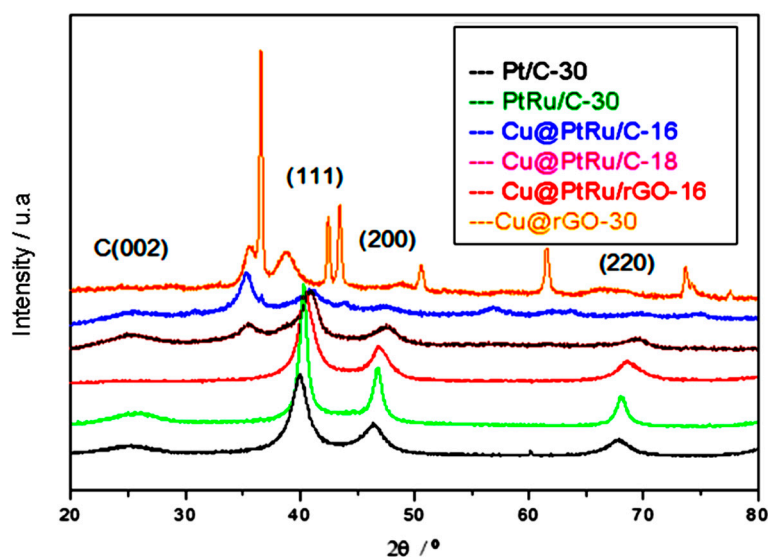


Figure 2. X-ray diffraction patterns of the Pt/C-30, PtRu/C-30, Cu@PtRu/C-16, Cu@PtRu/C-18, Cu@PtRu/rGO-16, and Cu/rGO-30 catalysts.

As observed in Figure 2, the crystallinity of Cu@PtRu/C is high, and the presence of peaks characteristic of the Pt structure suggests that the layer covering the core is formed, or specifically, in this case, implies that the estimated thickness of the PtRu alloy on the surface of Cu nanoparticles is higher than 1 nm [38,39]. The reason for the belief that the Cu@PtRu/rGO-16 nanoparticles (NPs) form a perfect core–shell system is the absence of the standard diffraction peaks characteristic of Cu atoms and their oxides at 2θ equal to 36° and 43° . The presence of these peaks for the Cu@PtRu/C-16 and Cu@PtRu/C-18 catalysts suggests that the coating of Cu NPs on these structures is only partial. The average size of the crystallites, determined via the Scherrer equation, is 3.6 nm (Cu/rGO), 3.8 nm (Pt/C-30), 3.4 nm (PtRu/C-30), 4.9 nm (Cu@PtRu/C-16), 4.4 nm (Cu@PtRu/C-18), and 4.5 nm (Cu@PtRu/rGO-16).

3.1.2. HRTEM Results

The core–shell structures have been also characterized via HRTEM, to allow comparison with the XRD results, and the visualization of changes in the distances among the crystallographic planes, due to the substitution of atoms on the NP surfaces that form the nuclei. Figure 3A–E display representative images obtained using HRTEM. From these images, a spherical shape is assumed for the Cu/rGO and Cu@PtRu/rGO-16 NPs, and a regular dispersion of these NPs on the rGO support is observed. The average diameter measured for the Cu/rGO NPs is 3.7 nm and, for the Cu@PtRu/rGO-16 NPs, is 4.9 nm, suggesting that a layer with a size of above 1 nm of PtRu is deposited on the surface of the Cu particles. The growth of the Pt alloys on the surface of the copper NPs can be

understood as an expansion of the copper crystal lattice, where, in general the outer layer is favored by two factors: the higher oxidation potential of the constituent metals of the core in relation to that of the metals in the covering layer, and this layer having the same crystalline arrangement of the core atoms [40,41].

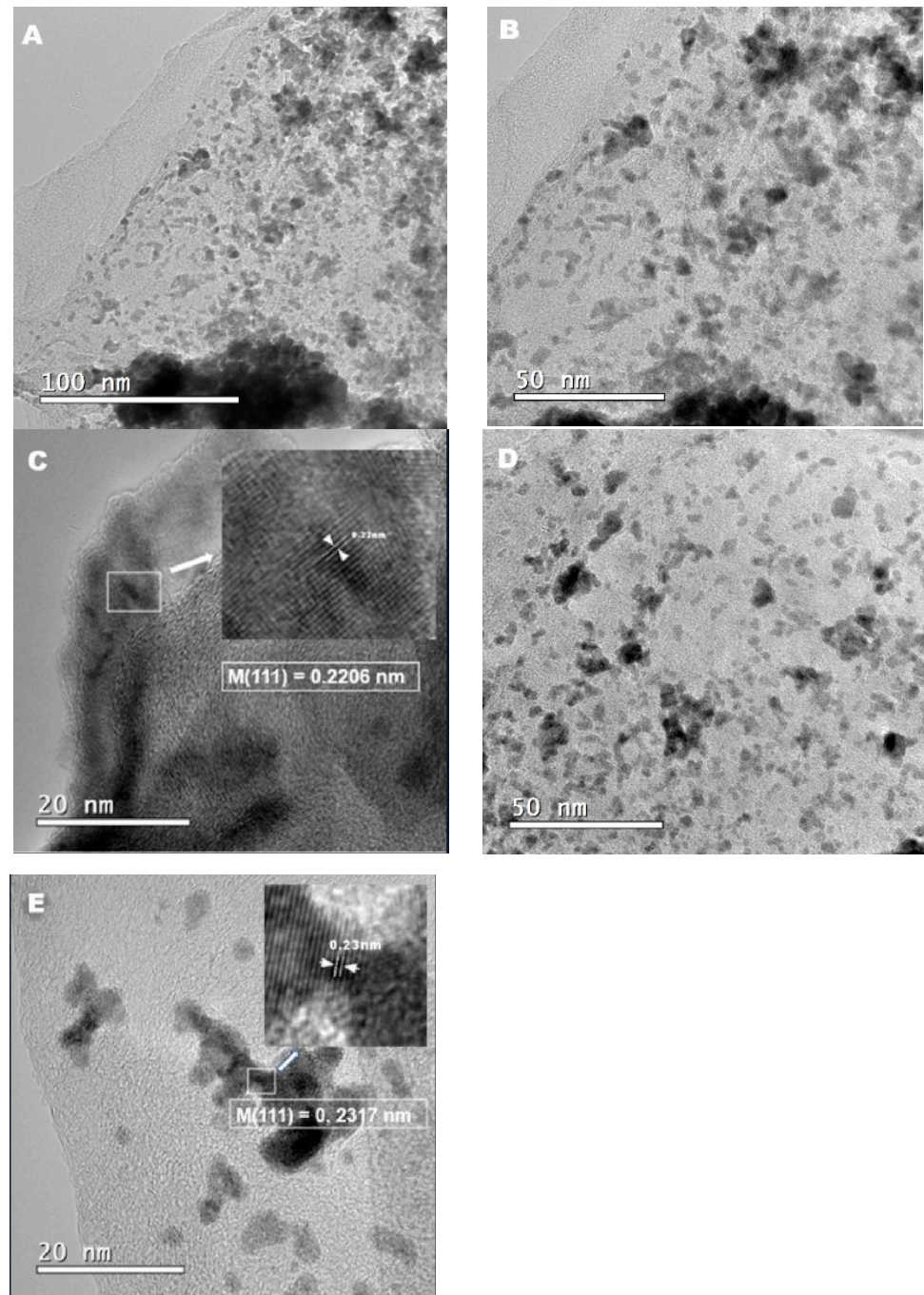


Figure 3. HRTEM images of Cu nanoparticles on rGO (A) and Cu@rGO (B). The interplanar distance of the FCC structure of copper (C). The increase in the interplanar distance, due to the PtRu coating (D). The formation of Cu@PtRu/rGO-16 (E).

The PtRu formation on Cu NPs is the result of charge transfer at the Cu/solution interface, and the increase in size, observed via HRTEM, in the Cu/rGO NPs is attributed to the reduction in Pt^{2+} and Ru^{3+} species. This reduction is favored over the Cu core, because the interaction between the metal ions and the copper atoms is stronger than

the interaction between them and the carbon support. Another factor favorable to the growth of the PtRu layer on the copper core is the crystalline arrangement of Pt and Cu, both FCCs. From Figure 3A,B, it is possible to observe, in darker contrast, the formation of agglomerates of Cu/rGO particles, resulting from the employed synthesis method. Regularly distributed regions are represented by NPs in a less-dark contrast. Figure 3D depicts a better distribution of the support for the Cu@PtRu/rGO-16 NPs, suggesting that the second step in the synthesis is the stage of the reconfiguration of the particle distribution on the support.

The brightness contrast between the core and shell regions observed in some Cu@PtRu/rGO NPs in Figure 3D is commonly attributed to the separation between the Cu core, the darker region, and the PtRu shell, the brighter region. However, the boundary between the core and the shell is not well defined in the images, and the separation between the phases is better defined via the measurement of the interplanar distance of the crystal constituting the core and, subsequently, the formed core–shell. The lattice planes of the Cu/rGO-30 NPs in Figure 3C exhibit an interplanar spacing of 0.2206 nm, corresponding to the (111) face of the copper alloy. In this case, a single particle is chosen arbitrarily. In Figure 3E, the distance measured between the two closest rows of atoms for the Cu@PtRu/rGO-16 NPs is 0.2317 nm, referring to the orientation of the (111) crystalline plane of the FCC structure of platinum. According to the XRD results that show the absence of the standard peaks characteristic of the copper crystal structure, it can be concluded that the distance between the planes in Figure 3E refers to the PtRu alloy. Eighty particles are randomly measured, to obtain the average particle size distribution of Cu@PtRu/rGO-16. The HRTEM results suggest that, in some cases, discrete Pt and PtRu particles are formed; however, this statement refers to a few measurements of particles showing sizes below the measured values for most Cu@PtRu/rGO-16 NPs obtained either via HRTEM or via the Scherer equation.

3.1.3. Cyclic Voltammetry Testing

The electrochemical performance of the Pt/C-30, PtRu/C-30 Cu@PtRu/C-16, Cu@PtRu/C-18, and Cu@PtRu/rGO-16 catalysts have been investigated via cyclic voltammetry in sulfuric acid, 0.5 mol L⁻¹ H₂SO₄, at 20 mV/s. The cyclic voltammograms of the catalysts are shown in Figure 4A–D. The current values for this cyclic voltammetry test have not been normalized. Each voltammogram is acquired after 22 cycles under a N₂ atmosphere, in order to obtain a more stable response from the electrode surface.

The electrocatalyst PtRu/C, and those with core–shell morphology Cu@PtRu/C-16, Cu@PtRu/C-18 and Cu@PtRu/rGO-16, show a poorly defined hydrogen adsorption/desorption region in the potential range of –0.2–0.15 V, versus Ag/AgCl, in relation to pure platinum. The poorly defined hydrogen adsorption region in the core–shell electrocatalysts may be related to the formation of surface ruthenium oxides at potentials lower than 0.15 V, versus Ag/AgCl, which may inhibit the hydrogen adsorption reaction on the platinum sites [42,43]. For the electric double-layer region (0.15 to 0.6 V), versus Ag/AgCl electrocatalysts, PtRu/C, Cu@PtRu/C-16, Cu@PtRu/C-18, and Cu@PtRu/rGO-16 present an enlargement of the electrical double layer in relation to the Pt/C catalyst, proving to be more capacitive, probably due to the increase in the number of pores and/or the reagglomeration of the sheets in the case of the core–layer morphology [44]. In general, the large surface area of Vulcan XC72R carbon and rGO favor a higher formation of oxygenated species, essential for methanol electrooxidation. The literature has shown that this enlargement of the voltametric profiles in the potential range of the double layer is characteristic of PtRu alloys, with platinum being the site of adsorption of electroactive species [45,46]. The small peak formed in the cathodic sweep at approximately 0.35 V, vs. Ag/AgCl, for all electrocatalysts corresponds to the reduction in oxides formed in the anodic sweep, and it can be noted that, contrary to what is observed in hydrogen adsorption/desorption, the redox potentials are not coincident, which shows the irreversible nature of this process. The current values of the cyclic voltammetry and chronoamperometry curves in 0.5 mol L⁻¹

H_3COH plus $0.5 \text{ mol L}^{-1} \text{ H}_2\text{SO}_4$ solution have been normalized, using the oxidation method of a CO monolayer adsorbed on the surface of all electrocatalysts.

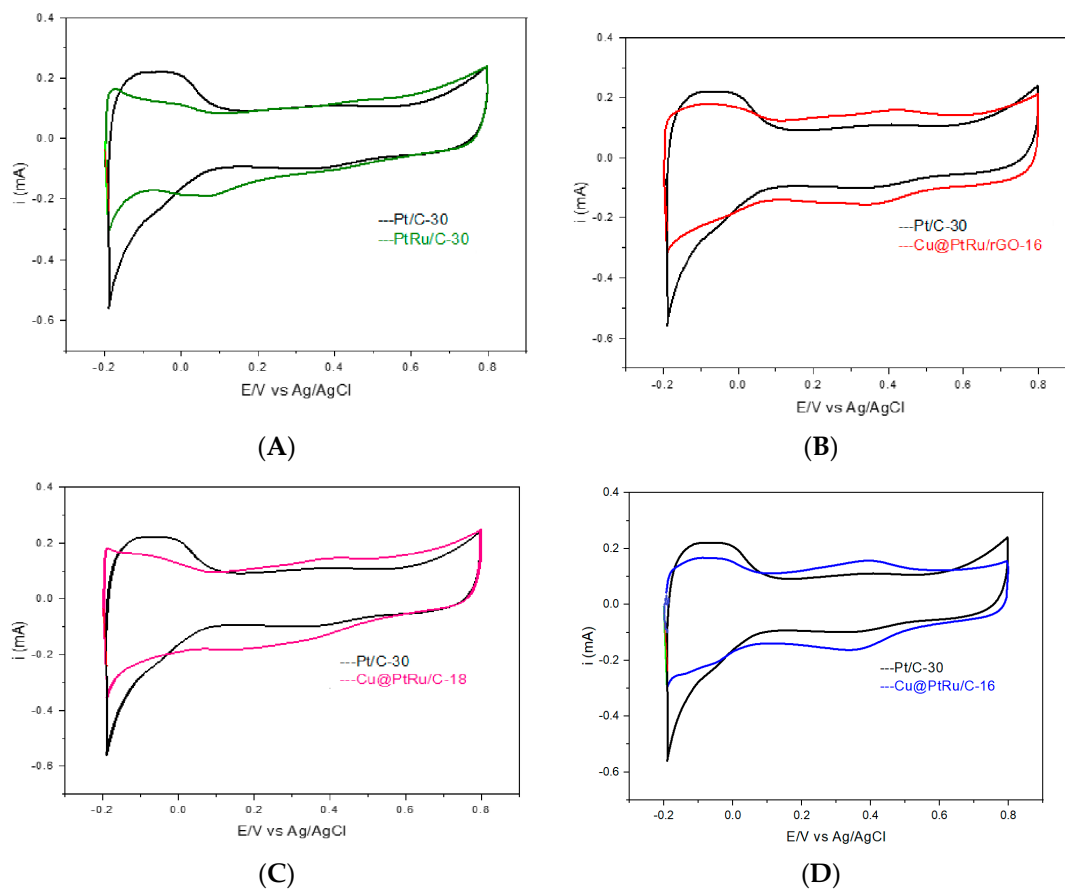


Figure 4. Cyclic voltammograms of Pt/C-30 and PtRu/C-30 (A), Pt/C-30 and Cu@PtRu/C-16 (B), Pt/C-30 and Cu@PtRu/C-18 (C), Pt/C-30 and Cu@PtRu/rGO-16 (D), obtained in a $0.5 \text{ M H}_2\text{SO}_4$ solution, at a scan rate of 20 mV/s .

In Figure 5A–D, the curves obtained for the anodic scans referring to the oxidation of methanol on the Pt/C-30, PtRu/C-30, Cu@PtRu/C-16, Cu@PtRu/C-18, and Cu@PtRu/rGO-16 electrocatalysts are superimposed. These curves have been obtained in solutions containing $0.5 \text{ M CH}_3\text{OH}$ plus $0.5 \text{ M H}_2\text{SO}_4$, at 20 mV/s , in the potential range between -0.2 and 0.8 V , vs. Ag/AgCl.

The anode scans in Figure 5 show that, for the low potential region (0.1 to 0.4 V), the Cu@PtRu/rGO-16 electrocatalyst depicts a higher current density value than the others. Similarly, its cyclic voltammograms in a $0.5 \text{ M H}_2\text{SO}_4$ solution show higher current density values. The second best is Cu@PtRu/C-16, followed by Cu@PtRu/C-18, both with a core-shell structure. Although the Cu@PtRu/C-16 and Cu@PtRu/C-18 catalysts depict lower current densities than that of Cu@PtRu/rGO-16, their current densities are higher than those of Pt/C-30 and PtRu/C-30.

The starting oxidation potential (SOP) is an important criterion used to evaluate and compare the catalytic activities of electrodes. The values measured for the SOP of each catalyst are shown in Table 1. The oxidation–reduction peaks of the Cu@PtRu/rGO-16 catalyst are lower than all the others. Cu@PtRu/C-16 and Cu@PtRu/C-18 have lower SOP values than those of Pt/C-30 and PtRu/C-30. The PtRu/C electrocatalyst, although it has a lower SOP value than that of Pt/C, has a higher value than the core–shell morphology electrocatalysts. Among the core–shells, Cu@PtRu/C-16 displays the lowest value in relation to Cu@PtRu/C-18. Among all the tested electrocatalysts, Cu@PtRu/rGO-16 exhibits the lowest SOP value, 0.250 V . Thus, the order of catalytic activities, according to the SOP value

criterion, is: Pt/C < PtRu/C-30 < Cu@PtRu/C-18 < Cu@PtRu/C-16 < Cu@PtRu/rGO-16. The better performance of the Cu@PtRu/rGO-16 electrocatalyst in relation to the others in methanol oxidation can be attributed to its high active surface, the higher number of oxygen-containing groups attached to the ruthenium atom (carboxyl, hydroxyl, etc.), the bifunctional mechanism, and the electronic effect; and to its efficient exfoliation process, or the higher thermal and mechanical stability of its carbon support [47,48]. The ratio between the forward (i_F) and reverse anodic (i_R) peak current densities can be used to describe the catalyst's tolerance to catalytic poison accumulation. A high i_F/i_R value indicates a more effective removal of species that poison the catalyst surface [37]. Table 1 shows the calculated values for i_F , i_R and i_F/i_R .

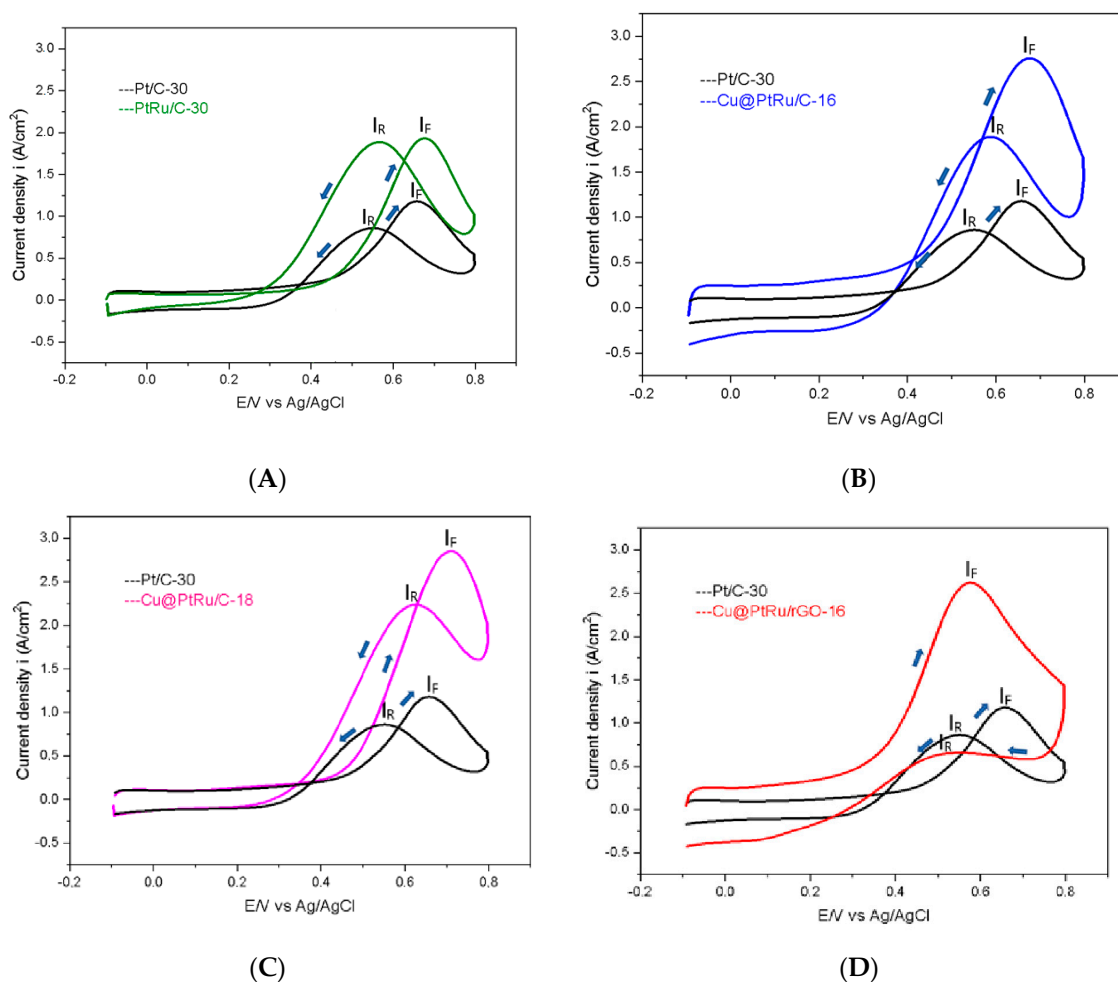


Figure 5. Anodic scans of Pt/C-30 and PtRu/C-30 (A), Pt/C-30 and Cu@PtRu/C-16 (B), Pt/C-30 and Cu@PtRu/C-18 (C), and Pt/C-30 and Cu@PtRu/rGO-16 (D) obtained in solution containing 0.5 M CH₃OH plus 0.5 M H₂SO₄, at 20 mV/s. Upward pointing blue arrows indicate forward anodic scanning, I_F. Blue arrows pointing down indicate anodic sweep backwards, I_B.

The Pt/C-30 (1.21 A/cm²) and PtRu/C-30 (1.96 A/cm²) electrocatalysts demonstrate the lowest i_F values in relation to Cu@PtRu/C-16 (2.79 A/cm²) and Cu@PtRu/C-18 (2.89 A/cm²). The i_F for the Cu@PtRu/rGO-16 electrocatalyst (2.68 A/cm²) is lower than that for the other core-shell systems; however, it possesses the lowest i_R (1.85 A/cm²) compared to the others, except for PtRu/C-30 (1.88 A/cm²). These results show that the Cu@PtRu/rGO-16 electrocatalyst has the highest i_F/i_R value (1.45 A/cm²) among all those studied here. In general, the i_F/i_R ratio is a measure of the efficiency of the bifunctional mechanism, and the electronic effect on the electrode kinetics.

Table 1. The starting oxidation potential (SPO) in volts, the forward peak current density (i_F) in Ampere per square centimeter, the reverse peak current density (i_R), and the i_F/i_R ratio for the Pt/C-30, PtRu/C-30, Cu@PtRu/C-16, Cu@PtRu/C-18, and Cu@PtRu/rGO-16 electrocatalysts, obtained via the reduction method.

Electrocatalyst	SOP (V)	i_F (A/cm ²)	i_R (A/cm ²)	i_F/i_R
Pt/C-30	0.437	1.21	0.99	1.22
PtRu/C-30	0.425	1.96	1.88	1.04
Cu@PtRu/C-16	0.300	2.79	2.02	1.38
Cu@PtRu/C-18	0.391	2.89	2.17	1.33
Cu@PtRu/rGO-16	0.250	2.68	1.85	1.45

3.1.4. Chronoamperometry Measurements for Methanol Electrooxidation

Chronoamperometric experiments have been carried out in a solution of 0.5 M methanol plus 0.5 M H₂SO₄, to observe the stability of the catalysts over time at a constant potential. The results are shown in Figure 6.

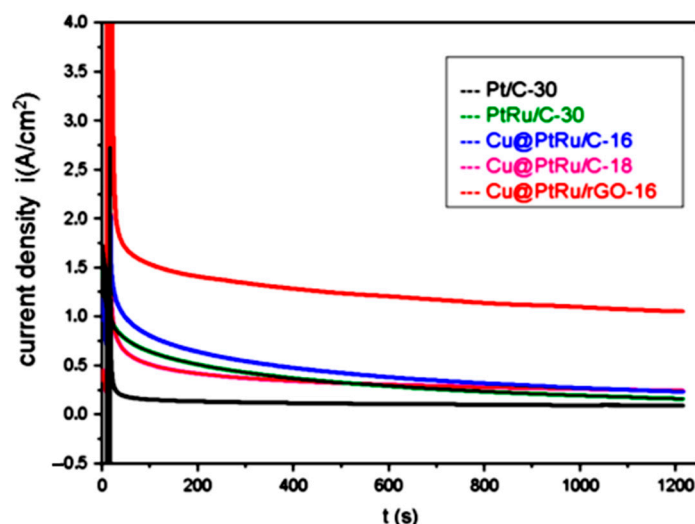


Figure 6. Chronoamperometric curves for the electrooxidation of methanol with Pt/C-30, PtRu/C-30, Cu@PtRu/C-16, Cu@PtRu/C-18, and Cu@PtRu/rGO-16, at 0.5 M of methanol plus 0.5 M H₂SO₄ solution, at the fixed potential of 500 mV.

The results obtained via chronoamperometry demonstrate that the PtRu/C-30, Cu@PtRu/C-16, Cu@PtRu/C-18, and Cu@PtRu/rGO-16 systems exhibit higher current density values than that of the standard Pt/C, after 20 min of operation, with a potential value of 500 mV. This fact is probably due to the bi-functional mechanism and/or the electronic effect resulting from the presence of ruthenium in the alloy. However, the core-shell electrocatalysts show a higher stability, and higher current density values than those of PtRu/C-30 and the conventional Pt/C-30, again indicating the beneficial effect of the core-shell structure in the electrocatalysts' performance. The current density value of the Cu@PtRu/rGO-16 catalyst is about four times higher than that of the Cu@PtRu/C-16 and Cu@PtRu/C-18 catalysts. In addition, it is about five times higher than that of the PtRu/C-30 catalyst, and around six times higher than that of Pt/C-30. These results suggest that Cu@PtRu/rGO-16 exhibits a high long-term bulk activity in methanol electrooxidation, a high stability, and a high tolerance to CO poisoning. The lower instability of the Cu@PtRu/C-16 and Cu@PtRu/C-18 catalysts may be related to the pseudo core-shell morphology that allows the presence of copper and its oxides on the surface of the NPs, which, according to the XRD results, does not take place with Cu@PtRu/rGO-16. The chronoamperometric results are further

supported by the HRTEM images that display a regular distribution of the NPs over the rGO support.

In the Cu@PtRu/C-16 and Cu@PtRu/C-18 electrocatalysts, the irregular formation of the layers that cover the core suggests that PtRu is reduced on the support in the form of a bimetallic alloy, or in the form of monatomic Pt and Ru alloys. In the latter case, the absence of the bifunctional mechanism, and the electronic effect on the dispersed Pt NPs significantly affect the performance of these catalysts. The following order of catalytic activities can be assigned approximately after 20 min of reaction: Pt/C < PtRu/C-30 < Cu@PtRu/C-18 < Cu@PtRu/C-16 < Cu@PtRu/rGO-16. The results obtained via chronoamperometry agree with those obtained via cyclic voltammetry in a 0.5 M H₂SO₄ solution, in the sense that the best electrocatalyst is Cu@PtRu/rGO-16, and the worst is Pt/C.

The higher current density values for Cu@PtRu/rGO-16 in relation to the other electrocatalysts suggest that the surface tension and other characteristic properties of the interface may be the cause of its better performance. This energy originating from the core–shell interface, as well as the electronic effect, may be associated with the weakening of the Pt-CO_{ads} bonds on the surfaces of the core–shell NPs. Thus, the free energy released at the phase boundary inside NPs with core–shell morphology, added to the electronic effect and the bi-functional mechanism, may be the cause of the greater tolerance to CO, and the consequent increase in the electrocatalytic activity of electrocatalysts with a core–shell morphology. The preponderance of one of these effects depends on the potential range considered. In fact, the increased tolerance of the PtRu alloy to CO has the effect of the preponderant ligand at potentials below 0.3 V, and the bifunctional mechanism at potentials above 0.3 V. The higher values of electrical current densities for Cu@PtRu/rGO-16 must be associated with the higher conductivity of rGO compared to Vulcan XC72R; thus, rGO support is crucial to the best performance of the Cu@PtRu/rGO-16 electrocatalyst.

4. Conclusions

In summary, it has been demonstrated that the core–shell/rGO combination is superior in catalytic activity to the traditional Pt/C, PtRu/C, and Cu@PtRu/C catalysts in the methanol oxidation reaction. The core–shell/rGO structure has been confirmed via XRD and HRTEM. The lower activity of the core–shell catalyst with an incomplete layer (pseudo core–shell), and supported on Vulcan carbon, is related to this partial encapsulation and the properties of the support. In the case of partial encapsulation, the formation of Pt crystals outside the PtRu alloy made its best use impossible. It is also concluded that the catalytic activity of the Cu@PtRu/C catalyst can indeed be improved via the use of rGO as a support, instead of Vulcan XC-72 carbon. Furthermore, considering that the Cu core significantly decreases the Pt loading on the catalyst, Cu@PtRu/rGO is a promising candidate material for large-scale fabrication in electrocatalysis. Cu@PtRu/rGO nanostructures have excellent catalytic properties, and their syntheses are simple, which paves the way for their utilization in fuel cell technologies.

Author Contributions: Conceptualization, W.d.S.G., J.P.I.d.S. and F.V.A.; Methodology, R.d.N.; Software, F.A.M.; validation, F.A.M. and J.P.I.d.S.; Formal analysis, W.d.S.G.; investigation, T.d.S.d.M. and W.d.S.G.; resources, F.A.M.; data curation, W.d.S.G.; writing—preparation of the original draft, W.d.S.G.; writing—proofreading and editing, J.P.I.d.S. and T.d.S.d.M.; visualization, J.P.I.d.S. and R.d.N.; supervision, R.d.N. and J.P.I.d.S.; project management, J.P.I.d.S.; financing acquisition, W.d.S.G. All authors have read and agreed to the published version of the manuscript.

Funding: This research received by PROPESP.

Data Availability Statement: We declare that all data used to prepare this manuscript are the result of experimental work and subsequent electrochemical and physical characterizations, and are authentic and not published elsewhere. Follow the link of the data obtained: https://drive.google.com/drive/folders/1ISHM-KINqtBYw61iHjlerleXi8rbwnUm?usp=drive_link (accessed on 17 August 2023).

Acknowledgments: The authors would like to thank Federal University of Pará and Capes for financial support. Additionally, the X-ray diffractometry and transmission electron microscope laboratories at the Chemistry Institute of São Carlos (USP) are grateful acknowledged, for the measurements.

Conflicts of Interest: The authors declare no conflict of interest.

References

1. Cheng, Y.; Zhang, J.; Lu, S.; Jiang, S.P. Significantly enhanced performance of direct methanol fuel cells at elevated temperatures. *J. Power Sources* **2020**, *450*, 227620. [[CrossRef](#)]
2. Sun, X.; Yang, C.; Xia, Z.; Qi, F.; Sun, H.; Sun, G. Molecular sieve as an effective barrier for methanol crossover in direct methanol fuel cells. *Int. J. Hydrogen Energy* **2020**, *45*, 8994–9003. [[CrossRef](#)]
3. Guo, J.; Zhang, M.; Xu, J.; Fang, J.; Luo, S.; Yang, C. Core-shell Pd-P@Pt-Ni nanoparticles with enhanced activity and durability as anode electrocatalyst for methanol oxidation reaction. *RSC Adv.* **2022**, *12*, 2246–2252. [[CrossRef](#)]
4. Pereira, P.A.; Andrade, J.B. Fontes, reactivity and quantification of methanol and ethanol in the atmosphere. *Quim. Nova* **1998**, *21*, 744–754. [[CrossRef](#)]
5. Liu, M.; Zhao, Z.; Duan, X.; Huang, Y. Nanoscale Structure Design for High-Performance Pt-Based ORR Catalysts. *Adv. Mater.* **2018**, *31*, 1802234. [[CrossRef](#)] [[PubMed](#)]
6. Abdelkareem, M.A.; Sayed, E.T.; Nakagawa, N. Significance of diffusion layers on the performance of liquid and vapor feed passive direct methanol fuel cells. *Energy* **2020**, *209*, 118492. [[CrossRef](#)]
7. Sekar, A.; Metzger, N.; Rajendran, S.; Elangovan, A.; Cao, Y.; Peng, F.; Li, X.; Li, J. PtRu Catalysts on Nitrogen-Doped Carbon Nanotubes with Conformal Hydrogenated TiO₂ Shells for Methanol Oxidation. *ACS Appl. Nano Mater.* **2022**, *5*, 3275–3288. [[CrossRef](#)]
8. Xu, H.; Shang, H.; Wang, C.; Du, Y. Recent Progress of Ultrathin 2D Pd-Based Nanomaterials for Fuel Cell Electrocatalysis. *Small* **2021**, *17*, 2005092. [[CrossRef](#)]
9. Mohanapriya, S.; Gopi, D. Microwave assisted synthesis of core-shell Ni-Co/graphene nanosheets and their catalytic activity for methanol electro-oxidation. *Mater. Today* **2022**, *51*, 1797–1881. [[CrossRef](#)]
10. Wang, X.; Li, H.; Feng, H.; Wang, H.; Lei, Z. Preparation of carbon-supported core@shell PdCu@PtRu nanoparticles for methanol oxidation. *J. Power Sources* **2010**, *195*, 1099–1102. [[CrossRef](#)]
11. Lee, D.; Gok, S.; Kim, Y.; Sung, Y.E.; Lee, E.; Jang, J.H.; Lim, T. Methanol Tolerant Pt-C Core-Shell Cathode Catalyst for Direct Methanol Fuel Cells. *ACS Appl. Mater. Interfaces* **2020**, *12*, 44588–44596. [[CrossRef](#)]
12. Salgado, J.R.C.; Alcaide, F.; Álvarez, G.; Calvillo, L.; Lázaro, M.J.; Pastor, E. Pt-Ru electrocatalysts supported on ordered mesoporous carbon for direct methanol fuel cell. *J. Power Sources* **2010**, *195*, 4022–4029. [[CrossRef](#)]
13. Christoffersen, E.; Liu, P.; Ruban, A.; Skriver, H.; Norskov, J. Anode Materials for Low-Temperature Fuel Cells: A Density Functional Theory Study. *J. Catal.* **2000**, *199*, 123–131. [[CrossRef](#)]
14. Sang, Y.; Zhang, R.; Xu, B.; Yang, J.; Zhao, C.; Xu, H. Ultrafine and Highly Dispersed PtRu Alloy on Polyacrylic Acid-Grafted Carbon Nanotube@Tin Oxide Core/Shell Composites for Direct Methanol Fuel Cells. *ACS Appl. Energy Mater.* **2022**, *5*, 4179–4190. [[CrossRef](#)]
15. Yola, M.L.; Eren, T.; Atar, N.; Saral, H.; Ermiş, İ. Direct-methanol Fuel Cell Based on Functionalized Graphene Oxide with Mono-metallic and Bi-metallic Nanoparticles: Electrochemical Performances of Nanomaterials for Methanol Oxidation. *Electroanalysis* **2015**, *28*, 570–579. [[CrossRef](#)]
16. Li, Y.; Gao, W.; Ci, L.; Wang, C.; Ajayan, P.M. Catalytic performance of Pt nanoparticles on reduced graphene oxide for methanol electro-oxidation. *Carbon* **2010**, *48*, 1124–1130. [[CrossRef](#)]
17. Lee, S.H.; Kakati, N.; Jee, S.H.; Maiti, J.; Yoon, Y.S. Hydrothermal synthesis of PtRu nanoparticles supported on graphene sheets for methanol oxidation in direct methanol fuel cell. *Mater. Lett.* **2011**, *65*, 3281–3284. [[CrossRef](#)]
18. Zhang, Y.; Guo, Z.; Zhu, H.; Xing, W.; Tao, P.; Shang, W.; Fu, B.; Song, C.; Hong, Y.; Dickei, M.D. Synthesis of Liquid Gallium@Reduced Graphene Oxide Core-Shell Nanoparticles with Enhanced Photoacoustic and Photothermal Performance. *J. Am. Chem. Soc.* **2022**, *144*, 6779–6790. [[CrossRef](#)]
19. Pan, J.; Li, S.; Zhang, L.; Yu, T.; Li, F.; Zhang, W.; Wang, J.; Zhang, D.; Yu, Y.; Li, X. Reduced Graphene Oxide/Ni Foam Supported ZIF-67 Derived CuCo₂S₄@CoS₂ Core-Shell Heterostructure for Boosted Electrochemical Energy Storage. *J. Energy Storage* **2022**, *47*, 103–112. [[CrossRef](#)]
20. Roh, G.; Lee, H.; Jeong, Y.; Kim, J.H. Preparation of Carbon-Supported PtRu Core-Shell Nanoparticles Using Carbonized Polydopamine and Ozone for a CO Tolerant Electrocatalyst. *Int. J. Hydrogen Energy* **2019**, *44*, 21588–21596. [[CrossRef](#)]
21. Wu, Y.N.; Liao, S.J.; Liang, Z.X.; Yang, L.J.; Wang, R.F. High-Performance Core-Shell PdPt@Pt/C Catalysts via Decorating PdPt Alloy Cores with Pt. *J. Power Sources* **2009**, *194*, 805–810. [[CrossRef](#)]
22. Patra, S.; Munichandraiah, N. Electrooxidation of Methanol on Pt-Modified Conductive Polymer PEDOT. *Langmuir* **2009**, *25*, 1732–1738. [[CrossRef](#)] [[PubMed](#)]
23. Szabó, T.; Berkesi, O.; Forgó, P.; Josepovits, K.; Sanakis, Y.; Petridis, D.; Dékány, I. Evolution of Surface Functional Groups in a Series of Progressively Oxidized Graphite Oxides. *Chem. Mater.* **2006**, *18*, 2740–2749. [[CrossRef](#)]

24. Wang, Z.; Hu, S.; Ali, A.; Chen, H.; Shen, P.K. Facile One-Pot Synthesis of a PtRh Alloy Decorated on Ag Nanocubes as a Trimetallic Core–Shell Catalyst for Boosting Methanol Oxidation Reaction. *ACS Appl. Energy Mater.* **2021**, *4*, 1085–1092. [[CrossRef](#)]
25. Hamnett, A. Mechanism and electrocatalysis in the direct methanol fuel cell. *Catal. Today* **1997**, *38*, 445–457. [[CrossRef](#)]
26. Yu, Y.; Chen, K.; Wu, Q.; Zhang, Y.; Shi, D.; Li, H. Recent progress on reduced graphene oxide supported Pt-based catalysts and electrocatalytic oxidation performance of methanol. *Int. J. Hydrogen Energy* **2023**, *48*, 1785–1812. [[CrossRef](#)]
27. Souza, J.P.L.; Queiroz, S.L.; Nart, F.C. Use of mass spectrometry in electrochemical measurements—The DEMS technique. *Quim. Nova* **2000**, *23*, 384–391. [[CrossRef](#)]
28. Iwasita, T.; Nart, F.C.; Vielstich, W. An FTIR Study of the Catalytic Activity of a 85:15 Pt:Ru Alloy for Methanol Oxidation. *Bunsenges. Phys. Chem.* **1990**, *94*, 1030–1034. [[CrossRef](#)]
29. Babu, P.K.; Kim, H.S.; Oldfield, E.; Wieckowski, A. Electronic Alterations Caused by Ruthenium in Pt-Ru Alloy Nanoparticles as Revealed by Electrochemical NMR. *Plenum* **1992**, *22*, 97–104. [[CrossRef](#)]
30. Mukerjee, S.; Urian, R.C. Bifunctionality in Pt alloy nanocluster electrocatalysts for enhanced methanol oxidation and CO tolerance in PEM fuel cell: Electrochemical and in situ synchrotron spectroscopy. *Electrochim. Acta* **2002**, *47*, 3219–3231. [[CrossRef](#)]
31. Hoster, H.; Iwasita, T.; Baumgartner, H.; Vielstich, W. Pt-Ru model catalysts for anodic methanol oxidation: Influence of structure and composition on the reactivity. *Phys. Chem. Chem. Phys.* **2001**, *3*, 337–346. [[CrossRef](#)]
32. Perrozzini, F.; Prezioso, S.; Ottaviano, L. Graphene oxide: From fundamentals to applications to cite this article. *J. Condens. Matter Phys.* **2015**, *27*, 013002. [[CrossRef](#)]
33. Hummers, W.S.; Offeman, R.E. Preparation of Graphitic Oxide. *J. Am. Chem. Soc.* **1958**, *80*, 1339. [[CrossRef](#)]
34. Frelink, T.; Visscher, W.; Cox, A.P.; Van Veen, J.A.R. Ellipsometry and dems study of the electrooxidation of methanol at Pt and Ru- and Sn-promoted Pt. *Electrochim. Acta* **1995**, *40*, 1537–1543. [[CrossRef](#)]
35. Antolini, E.; Cardellini, F. Formation of carbon supported PtRu alloy: An XRD analysis. *J. Alloys Compd.* **2001**, *315*, 118–127. [[CrossRef](#)]
36. Mcbreen, J.; Mukerjee, S. In situ X-ray Absorption Studies of a Pt-Ru Electrocatalyst. *J. Electrochem. Soc.* **1995**, *142*, 3399–3404. [[CrossRef](#)]
37. Wang, H.; Wang, R.; Li, H.; Wang, Q.; Kang, J.; Lei, Z. Facile synthesis of carbon-supported pseudo-core@shell PdCu@Pt nanoparticles for direct methanol fuel cells. *Int. J. Hydrogen Energy* **2011**, *36*, 839–848. [[CrossRef](#)]
38. Muthuswamy, N.; La Fuente, J.L.G.; Dung, T.; Walmsley, J.; Tsyppkin, M.; Raaen, S.; Sunde, S.; Ronning, M.; Chen, D. Ru@Pt core-shell nanoparticles for methanol fuel cell catalyst: Control and effects of shell composition. *Int. J. Hydrogen Energy* **2013**, *38*, 16631–16641. [[CrossRef](#)]
39. Wu, Q.; Huang, X.; Wang, T.; Xiang, D.; Li, X.; Wang, K.; Yuan, X.; Li, P.; Zhu, M. Enhancing Electrocatalytic Methanol Oxidation on PtCuNi Core–Shell Alloy Structures in Acid Electrolytes. *Inorg. Chem.* **2022**, *61*, 2612–2618. [[CrossRef](#)]
40. Zhu, H.; Li, X.; Wang, F. Synthesis and characterization of Cu@Pt/C core-shell structured catalysts for Exchange membrane fuel cell. *Int. J. Hydrogen Energy* **2011**, *36*, 9151–9154. [[CrossRef](#)]
41. Liu, H.; Sun, F.; Chen, M.; Wang, H. Reconciling the experimental and computational methanol electro-oxidation activity via potential-dependent kinetic mechanism analysis. *J. Mater. Chem. A* **2022**, *10*, 23551–23561. [[CrossRef](#)]
42. Hsin, Y.L.; Hwang, K.C.; Yeh, C.T. Poly(vinylpyrrolidone)-Modified Graphite Carbon Nanofibers as Promising Supports for PtRu Catalysts in Direct Methanol Fuel Cells. *J. Am. Chem. Soc.* **2007**, *129*, 9999–10010. [[CrossRef](#)]
43. Smith, A.S.; Lachance, A.M.; Zeng, S.; Liu, B.; Sun, L. Synthesis, properties, and applications of graphene oxide/reduced graphene oxide and their nanocomposites. *Nano Mater. Sci.* **2019**, *1*, 31–37. [[CrossRef](#)]
44. Neto, A.O.; Linardi, M.; Gonzales, E.R. Electrochemical oxidation of methanol on PtRu and PtMo particles supported on high surface area carbon. *Eclat. Quim.* **2003**, *28*, 55–62. [[CrossRef](#)]
45. Mekazni, S.D.; Arán-Ais, R.M.; Ferre-Vilaplana, A.; Herrero, E. Why Methanol Electro-oxidation on Platinum in Water Takes Place Only in the Presence of Adsorbed OH. *ACS Catal.* **2022**, *12*, 1965–1970. [[CrossRef](#)]
46. Baomin, L.; Qiang, Z.; Yezhen, Z.; Lijuan, W.; Fenfen, L.; Haiquan, X. Core-shell Ag nanowires@Pt nanorods catalyst: Synthesis and application in direct methanol fuel cells. *Mater. Lett.* **2018**, *233*, 138–141. [[CrossRef](#)]
47. Watanabe, M.; Motoo, S. Electrocatalysis by ad-atoms—Part II: Enhancement of the oxidation of carbon monoxide on platinum by ruthenium ad-atoms. *J. Electroanal. Chem. Interfacial Electrochem.* **1975**, *60*, 267–273. [[CrossRef](#)]
48. Rigsby, M.A.; Zhou, W.P.; Lewera, A.; Duong, H.T.; Bagus, O.S.; Jaegermann, W.; Hunger, R.; Wieckowski, A. Experiment and Theory of Fuel Cell Catalysis: Methanol and Formic Acid Decomposition on Nanoparticle Pt/Ru. *J. Phys. Chem. C* **2008**, *112*, 15595–15601. [[CrossRef](#)]

Disclaimer/Publisher’s Note: The statements, opinions and data contained in all publications are solely those of the individual author(s) and contributor(s) and not of MDPI and/or the editor(s). MDPI and/or the editor(s) disclaim responsibility for any injury to people or property resulting from any ideas, methods, instructions or products referred to in the content.